

<https://doi.org/10.1038/s42005-024-01654-1>

Si-CMOS compatible epsilon-near-zero metamaterial for two-color ultrafast all-optical switching

Check for updates

Alessandro Pianelli ¹, Rakesh Dhama ¹, Jarosław Judek ², Rafał Mazur³ & Humeyra Caglayan ¹ ✉

Driven by the escalating demands of advanced technologies, developing integration strategies has kept pace with the realization of ultrafast components during the past two decades. Ultrafast all-optical switches enabled by artificial materials are considered at the forefront of the next generation of photonic integration for communications and high-volume data processing. Encouraged by these advancements, applications, and interest have increased toward all-optical switches based on epsilon-near-zero (ENZ) materials. However, some all-optical switches lack CMOS compatibility, require high energy activation, and are limited in switching speed and working wavelength. Here, we propose and demonstrate a multilayered ENZ metamaterial utilizing Si-compatible titanium nitride and indium-tin-oxide materials with two effective working wavelengths in the visible and near-infrared spectrum. This device enables switching time down to a few hundred femtoseconds utilizing minimal energy at the corresponding ENZ regions induced by intraband pumping. Our approach can enhance the adaptability of designing ENZ metamaterials for new hybrid integrated photonic components for low-power ultrafast all-optical terahertz modulation.

Over the past decade, the rapid advancement of information communications technology has led us to a significant demand for such efficient devices that can operate at high speed and large capacity. Today's data processing devices, which mainly rely on integrated electronic circuits, suffer from high power consumption and heat while functioning. Replacing these circuits at network nodes with ultralow-energy, ultrasmall, and fast switches as all-optical data-processing elements is the key to future interconnect technology¹. Photonics-based all-optical devices can play a vital role in this progress, enabling high bit rate data transmissions at low cost, reduced power consumption, and smaller footprints.

All-optical switches enable the ON/OFF conversion function by following the concept of light-controlled-by-light. They are highly significant due to their potential to overcome speed limitations set by electrical switches^{2–6}. Such an all-optical switching approach is the basis of the solid foundation for novel applications in optical communication networks, optical computing systems, quantum information processing chips, and photonic central processing units^{7–9}. This switching method mainly relies on the third-order nonlinearities of optical materials and their response time, making these materials with optimum nonlinear properties crucial for ultrafast switching devices. In this regard,

several different approaches based on photonic crystals¹⁰, plasmonic metamaterials^{11,12}, phase change materials¹³, two-dimensional (2D) materials², and hybrid perovskite materials¹⁴ have been reported for the realization of ultrafast all-optical switches, yet to provide a good solution.

Epsilon-near-zero (ENZ) materials^{15,16} emerge as one of the promising materials for realizing ultrafast all-optical devices with nonlinear properties. ENZ materials, whose dielectric permittivity takes extremely low values^{17–19} and eventually vanishes at a specific range of wavelengths, are very efficient at modulating the refractive index at the femtosecond (fs) scale^{20–22}. In the realm of all-optical switching systems, ENZ materials offer several benefits^{16,17}. Such materials provide a foundation for efficient optical switching capabilities at low activation energy due to the enhanced light-matter interaction in the ENZ region. Moreover, their miniaturization and integration possibilities usher towards a new era of compact and embedded optical components. ENZ metamaterials further reduce the phase mismatch between optical pulses and the ENZ medium, thereby improving nonlinearities. Another relevant benefit is the ENZ medium's ability to mitigate group velocity dispersion, ensuring minimal distortion as short pulses propagate in the ENZ media.

¹Faculty of Engineering and Natural Sciences, Tampere University, Korkeakoulunkatu 7, Tampere 33720, Finland. ²Institute of Microelectronics and Optoelectronics, Warsaw University of Technology, Koszykowa 75, Warsaw 00-662, Poland. ³Institute of Applied Physics, Military University of Technology, ul. gen. Sylwestra Kaliskiego 2, Warsaw 00-908, Poland. ✉e-mail: humeyra.caglayan@tuni.fi

Therefore, this opens up a new paradigm for photonic applications taking advantage of the linear and nonlinear properties^{33–29}. In particular, Si-compatible ENZ materials that can be integrated with silicon photonics circuits significantly reduce the cost and manufacturing complexities. This would provide more efficient performance and new functionalities in hybrid integrated photonics devices concepts, i.e., logic analysis^{28,30}. In this respect, transparent conducting oxides (TCOs) that are complementary metal oxide semiconductor (CMOS) compatible, such as indium-tin-oxide (ITO) and aluminum-doped zinc oxide (AZO), turn out to be relevant homogeneous ENZ materials operating at the telecom window as ultrafast photonics components^{15,16,20,31,32}. However, these materials are limited by their intrinsic optical properties, and a tailorable ENZ is needed to enable ultrafast switches, particularly at the wavelengths of interest.

Other than the homogeneous materials, subwavelength multilayer structures, often called hyperbolic metamaterials (HMMs)^{33–39}, are suitable candidates to design ENZ regime even towards visible wavelengths^{40,41}. Such layered structures have been envisioned as a potential new avenue for nonlinear optics because of their high nonlinear effective susceptibility⁴². The enhancement of nonlinear properties in the layered structures⁴³ and their nonlinearities have been theoretically analyzed in the framework of homogenized approximation⁴⁴. There have been quite extensive works that mainly focus on the ultrafast nonlinear response in ENZ materials as well as effective ENZ multilayered structures like HMMs^{15,16,45–49}. HMMs have proven to be excellent media for providing ultrafast optical switching in their effective ENZ^{45,46}. In particular, HMM-based on Ag/SiO₂ bilayers provides high nonlinear response with relatively fast (≈ 1 ps) response times⁵⁰. Recently, a remarkably high third-order nonlinearity on the order of 10^{-9} cm²/W at the effective ENZ regime in an HMM composed of Au/Al₂O₃ bilayers was demonstrated⁵¹. Encouraged by these developments, to enable the integration of the ENZ materials into the photonic chips, several drawbacks of ENZ materials need to be overcome, for instance: (i) tailoring the effective ENZ at the wavelength of interest to achieve broadband or multiple wavelength ranges, (ii) the use of quite low-loss materials, and (iii) Si-compatible materials.

To address these criteria, this work proposes a multilayer metamaterial designed with two Si-compatible materials, i.e., titanium nitride (TiN) and ITO. The HMM with four bilayers possesses two-color ENZ, i.e., ENZ in visible and near-IR ranges (telecom windows spanning from O- to S-band). Using the pump and probe transient absorption spectroscopy (TAS) technique, we investigated the ultrafast optical response of the HMM in its effective ENZ wavelengths, unveiling all-optical switching response times as short as a few hundred femtoseconds (fs) to surpass the performance of the ENZ Terahertz modulator counterpart^{15,16,52,53}. Figure 1 depicts the concept

of the two-color all-optical ultrafast switching epsilon-near-zero meta-device. The absorption responses of the HMM per unit volume in each building block in the stack are also shown in the inset of the figure for pump VIS- (700 nm) and NIR-ENZ (1250 nm) wavelengths (see the methods section for absorption calculations). The HMM can simultaneously support multiple ultrafast switches capable of all-optically modulating the response at distinct ENZ wavelengths. Such all-optical modulation renders this particular meta-device an ideal candidate for unlocking unique functionalities and new possibilities in integrated photonic switches.

Results and discussion

As the first step, TiN and ITO layers were separately deposited by magnetron sputtering and electron beam evaporation on float glass substrates ($n = 1.45$), respectively. The optical constants (refractive index (n) and extinction coefficient (k)) of these films were retrieved by performing spectroscopic ellipsometry, as shown in Supplementary Note 1. These data have been further utilized in Ansys Lumerical software to perform numerical simulations and design the desired HMM. In this context, four bilayers of TiN and ITO stacked films theoretically provide an HMM structure that enables two ENZ resonances. Thus, the final HMM structure has been realized by alternatively depositing the TiN (11 nm) and ITO (32 nm) up to four bilayers to obtain ENZ at two different wavelength regions, i.e., visible and near-infrared, as shown in the Supplementary Note 1. Figure 2a shows the effective real and imaginary parts of the permittivities responses of the HMM in the visible and near-IR ranges, which is calculated in the framework of effective media theory based on experimentally obtained dielectric permittivities ϵ_{TiN} , ϵ_{ITO} and thicknesses of the TiN and ITO layers L_{TiN} and L_{ITO} ³⁵. The wavelength region at which the parallel permittivity ϵ_{\parallel} crosses zero (from +1 to -1) falls in the range of 649–810 nm and is referred to as the visible epsilon-near-zero (VIS-ENZ) region. Additionally, the real part of the perpendicular permittivity ϵ_{\perp} vanishes in the range from 1238 to 1500 nm and is named the near-infrared ENZ (NIR-ENZ) region. Thus, ultrafast switching is expected within these ENZ regions. Note that the imaginary parts of the permittivities in both ENZ regions are $\text{Im}(\epsilon_{\parallel}) = 1.4$ and $\text{Im}(\epsilon_{\perp}) = 0.4$.

The appearance of these two ENZ regions is clearly shown in the calculated reflection spectrum (see the dashed regions of Fig. 2b). One can observe that the VIS-ENZ region is present at each incident angle till approx 70°. In contrast, the NIR-ENZ region begins to appear when the HMM is illuminated with an impinging angle above 40° degree, achieving the maximum at an angle of 70° degree. Furthermore, Fig. 2c shows good agreement of the HMM transmission and reflection curves between experimental results and simulations obtained via the Finite-difference

Fig. 1 | Two-color all-optical ultrafast switching in epsilon-near-zero multilayer metamaterials: concept and simulated absorption. **a** Schematic concept of the two-color all-optical ultrafast switching epsilon-near-zero multilayer metamaterials along with the simulated absorption of the HMM in the VIS and NIR regions, investigate with pump Intra-band Excitations of 700 nm and 1250 nm, respectively. **b** Represents the transient response of several classes of materials such as Semiconductors (green line) TCOs (light brown line), and metals (magenta line), showing that TiN/ITO HMM (Nitride/TCOs, cyan line) can provide a faster switch time performance as demonstrated in this work.

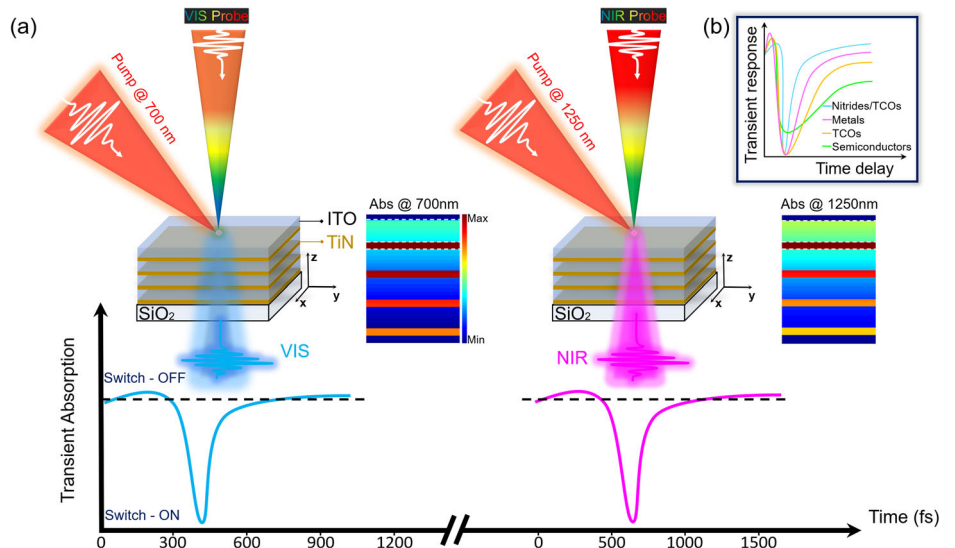
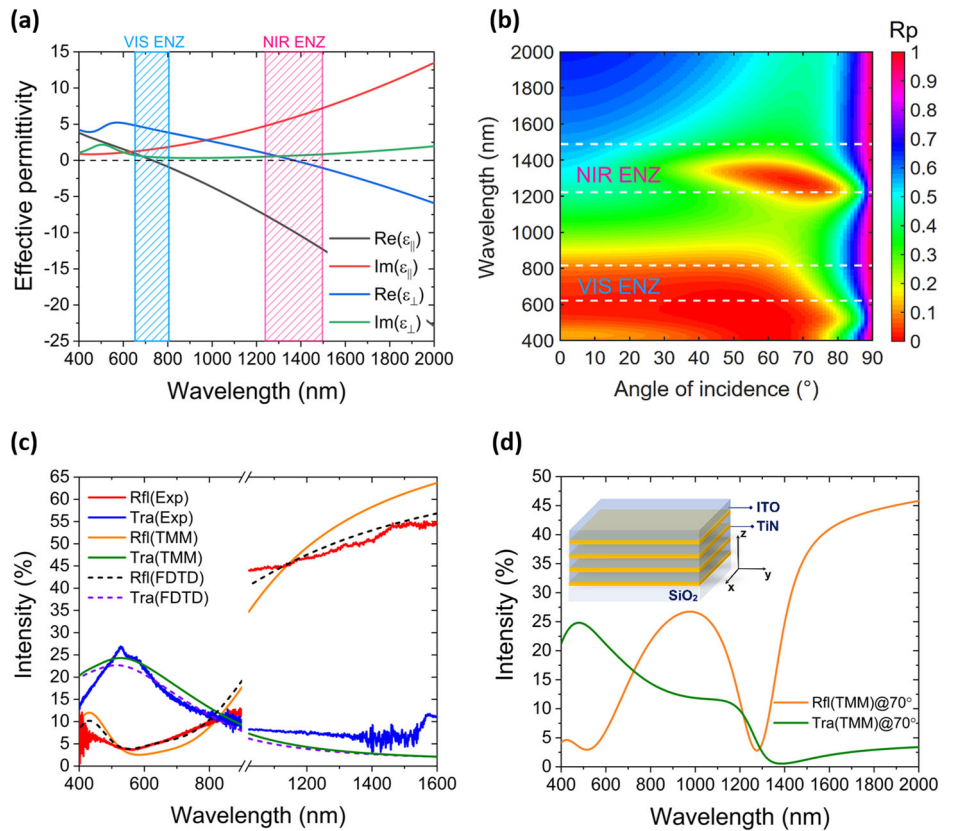


Fig. 2 | Linear characterization and analysis of TiN/ITO-based HMM. **a** Effective real and imaginary parts of permittivities of TiN/ITO based HMM, **b** calculated p-polarized reflection spectrum via the TMM method showing ENZ region in visible (VIS) and near-IR (NIR) as a function of the angle of incident light (θ). **c** Experimental and numerically simulated reflection and transmission curves of HMM by using FDTD and TMM methods at normal incidence. **d** Reflection and transmission curves at the excitation of 70° angle of the incident light, while the inset depicts the sketch of the engineered HMM.



time-domain (FDTD) and Transfer-matrix method (TMM), thus ensuring the experimental validation of the HMM. While Fig. 2d presents the typical NIR-ENZ regime response with 70° incident angle accordingly with the p-polarized reflection distribution in Fig. 2b. This response is also typically observed in ENZ materials films⁵⁴. In addition, s-polarized transmission and reflection responses of the investigated HMM are also reported in the Supplementary Note 1.

Ultrafast switching response

In order to investigate the switching mechanism in VIS-ENZ and NIR-ENZ regimes, HMM was excited by different intraband pump wavelengths and probed in the visible and near-infrared regions utilizing transient absorption spectroscopy (TAS) in transmission mode. A pump beam with less than 100 fs pulse duration excites the system, and probe pulses are delayed with respect to pump pulses to ascertain the spatial and temporal dynamics of the two-color HMM in the wavelength region of interest. In particular, we emphasized transient modulation at intraband excitation in the corresponding ENZ regions as it induces highly non-thermal electrons, i.e., hot electrons (HEs) at lower energy consumption^{16,55} and enables relaxation dynamics of HEs at ultrafast sub-picosecond scale. Furthermore, transient absorption (TA) experiments have also been conducted to investigate switching responses within one ENZ region upon the excitation of intraband excitation of other ENZ regions and vice versa.

To understand the change in switching time response of the VIS-ENZ region due to the incident angle of the pump beam, we first excited the HMM at normal incidence and 70° incidence angle by 700 nm (1.7 eV) pump wavelength with a fluence of $1.40 \text{ mJ} \cdot \text{cm}^{-2}$ and probed in visible (420–800 nm) region. Throughout our study, we maintained quite a low fluence in comparison to existing works within the realm of ultrafast ENZ at the THz switching speed^{6,15,16,20,45,52,53,56}. Figure 3a, b shows the 2D color maps of transient absorption (ΔA) as the function of wavelength and time at the normal incidence and 70° angle of the incident pump pulses, respectively. Similarly, the TA spectra are reported as a function of wavelength at

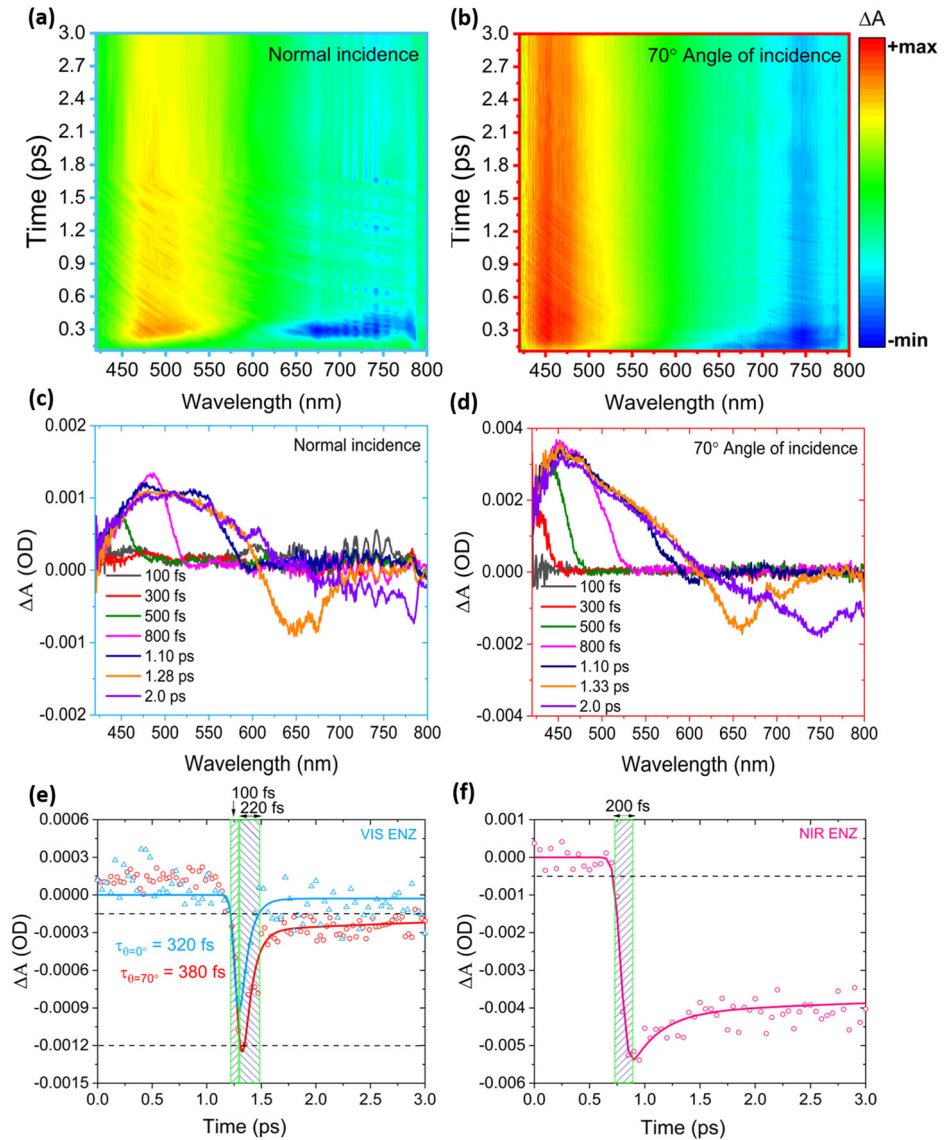
different time delays, as shown in Fig. 3c, d. It is clearly visible from Fig. 3 that oblique (70° angle) incidence of pump pulses enables stronger transient response in comparison to normal incidence, and the system undergoes a transition from excessive absorption maxima (positive ΔA) to negative transient absorption (bleach) region within sub-picosecond time scale. This short-lived state (the so-called Bleaching), which generally occurs at the resonance or at the ENZ of the considered system, is the temporal attenuation of the absorption caused by the photoinduced transition of the electrons to unoccupied higher energy states. While in this particular HMM, the promotion of electrons to higher energy levels has its strongest effect on the transient ultrafast dynamics where the free-carrier absorption is dominant at the cross-over frequency (ENZ)⁵⁵.

Such an ultrafast transition from positive transient absorption to bleach region in ENZ media indicates the presence of optical switching at a few hundred femtoseconds time scale.

Three processes can mainly describe the physical phenomena behind such all-optical intraband ultrafast switching in HMM. (i) In the absence of pump pulses, electrons of both building blocks are in the conduction band at their equilibrium state defined by Fermi distribution. (ii) After the pump pulse impinges the HMM, the electrons in the conduction band are energized, which quickly equilibrate via electron-electron (e-e) and electron-phonon (e-p) scattering described by a quasi-Fermi dynamics, leading to the creation of a highly non-thermal distribution at a well-defined elevated temperature^{56,57}. (iii) Hot electrons dissipate energy through e-p interactions, increasing the lattice temperature until the system returns to its initial equilibrium state. This process is associated with the switching off-recovery time. In general, the ultrafast relaxation time of HEs occurs at a rate mainly governed by the electron-phonon (e-p) coupling over a timescale of femtoseconds to picoseconds and induced charge dynamics in the systems^{16,52,58}.

We further studied the temporal dynamics of transient absorption of HMM in the VIS-ENZ region at normal incidence and 70° angle of incidence of pump and probe lights when excited by VIS-ENZ wavelength (700 nm pump pulses) under a similar pump fluence ($1.40 \text{ mJ} \cdot \text{cm}^{-2}$). Note

Fig. 3 | Temporal dynamics and spectral response of TiN/ITO-based HMM under intraband excitation (700 nm). 2D color maps of transient absorption as a function of wavelength and pump-probe delay time, when excited by 700 nm pump wavelength with a fluence of $1.40 \text{ mJ} \cdot \text{cm}^{-2}$ (a) at the normal incidence and (b) at 70° angle of the incident pump pulses. Transient absorption (ΔA (OD)) spectra curves at specific time delays (c) at normal incidence and (d) at 70° angle of the incidence, extracted from a and b, respectively. e Switching time responses of TiN/ITO-based HMM with excitation of 700 nm with a fluence of $1.40 \text{ mJ} \cdot \text{cm}^{-2}$ probed at 650 nm (VIS-ENZ) for normal incidence (blue line) and 70° angle of incidence (red line). Rise time is $100 \pm 13 \text{ fs}$ and fall time is $220 \pm 17 \text{ fs}$ (blue line), fall time is $280 \pm 26 \text{ fs}$ (red line). f Switching time responses at 1240 nm (NIR-ENZ) with 70° angle of incidence. Rise time is $200 \pm 16 \text{ fs}$, fall time is $78 \pm 6.4 \text{ ps}$ (Supplementary Fig. S10, Supplementary Note 4). Note that in e and f, full lines represent the kinetics fit of the experimental data illustrated by triangles and circles.



the fitting equation used for kinetic curves (solid line in the Figures of temporal dynamics) is mentioned in the methods section. Figure 3e visualizes the kinetic curves as the function of pump-probe delay time extracted from Fig. 3a, b at normal and oblique incidence to compare the switching time responses in both cases. Despite the stronger transient response under oblique incidence, HMM exhibits a faster switching time (blue curve) at normal incidence ($\tau_{\theta=0^\circ} = 320 \text{ fs}$) in comparison to the switching time (red curve) at 70° angle of incidence ($\tau_{\theta=70^\circ} = 380 \text{ fs}$) for the transition wavelength of VIS-ENZ region (650 nm), as shown in Fig. 3e. In the Supplementary Note 2, we report the switching time of Fig. 3e, for normal incidence, in terms of transmittance change over time ($\Delta T/T$), as illustrated in Supplementary Fig S7a.

Furthermore, the temporal dynamics of transient response in the NIR-ENZ region of HMM were investigated when excited at the intraband transition of the VIS-ENZ region under similar experimental conditions. Figure 3f reports a resolution-limited rise time of 200 fs, followed by a long-lasting tail response indicating more extended relaxation dynamics. Fast time (200 fs) at sub-ps scale in such a dynamic behavior is attributed to those HEs which relax through internal non-radiative relaxation processes, transforming from non-thermal to thermal energy distribution via electron-electron (e-e) scattering. Whereas the long-tail represents the slow dynamics due to the heat released from the lattice to the surrounding environment via

phonon-phonon (p-p) scattering within a time scale from hundreds of picoseconds to nanoseconds^{59,60}. Indeed, if we expand the probe temporal delay time window to 200 ps, the heat of the lattice is mainly released via the phonon-phonon (p-p) scattering process with a relaxation time of $\approx 78 \text{ ps}$, as shown in Supplementary Fig. S10 of the Supplementary Note 4.

In addition, we investigated the switching performance of HMM in both ENZ regions when pumped at the intraband excitation wavelength of the NIR-ENZ region at 70° angle of incidence. In this regard, Fig. 4a shows the temporal dynamics of transient modulation for 783 nm probe wavelength at the excitation of 1250 nm NIR pump pulses with a lower fluence of $1.16 \text{ mJ} \cdot \text{cm}^{-2}$. Note, the switching contrast and time-dependent optical response with high fluence values become quite irrelevant, particularly in the context of ultrafast processes involving Nitrides⁶¹. This is because Nitrides exhibit weak sensitivity to pump fluence⁵⁶.

The metadvice undergoes an ultrafast bleach response time of 160 fs, followed by a recovery process that takes 390 fs to return to its partially recovered state as shown in Fig. 4a. After this ultrafast temporal dynamics, a long-tail feature remains constant for several hundred picoseconds. This behavior is known as a "fast" and "slow" contribution of the relaxation time typically featured in TiN films in contrast to the gold switching dynamics⁶². Hence, the 'fast' component is dictated by the generated hot electrons. This process is generally observed within the time scale of 200 fs, during which

Fig. 4 | Switching responses in VIS and NIR-ENZ with Intraband Excitation (1250 nm). Switching time responses of HMM by intraband excitation of NIR-ENZ region (1250 nm) with the pump fluence of $1.16 \text{ mJ} \cdot \text{cm}^{-2}$, at 70° angle of incidence. **a** In VIS-ENZ at 783 nm probe wavelength, the rise time is $160 \pm 26 \text{ fs}$, and the fall time is $230 \pm 37 \text{ fs}$. **b** In the NIR-ENZ region at 1325 nm probe wavelength, the rise time is $60 \pm 6.6 \text{ fs}$, and the fall time is $480 \pm 43 \text{ fs}$. Full lines represent the kinetics fit of the experimental data illustrated by circles.

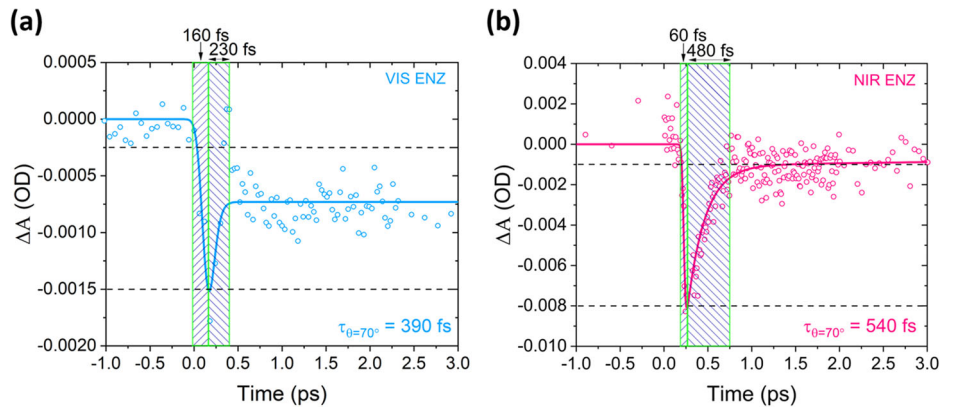
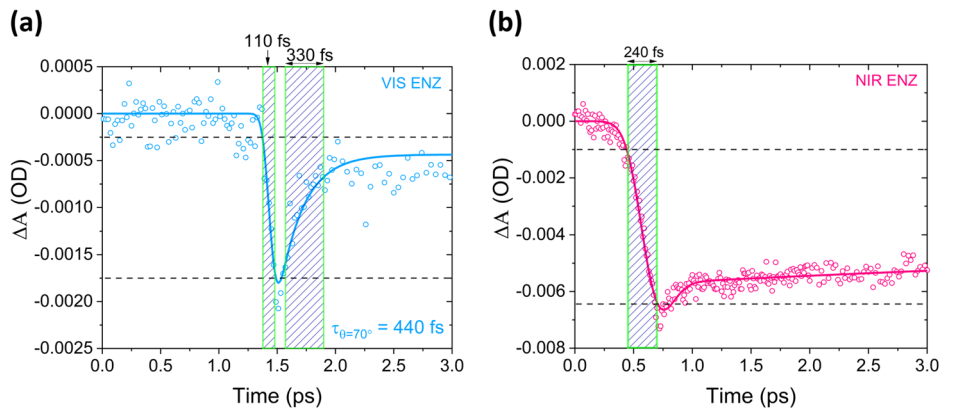


Fig. 5 | Switching responses in VIS and NIR-ENZ with Intraband Excitation (400 nm). Switching time responses of HMM with excitation of 400 nm pump pulses with a fluence of $1.40 \text{ mJ} \cdot \text{cm}^{-2}$, at 70° angle of incidence in **a** VIS-ENZ at 650 nm probe wavelength, the rise time is $110 \pm 15 \text{ fs}$ and the fall time is $330 \pm 34 \text{ fs}$. **b** In the NIR-ENZ region at 1240 nm probe wavelength, the rise time is $240 \pm 61 \text{ fs}$, and the fall time is $110 \pm 1.7 \text{ ps}$ (Supplementary Fig. S11, Supplementary Note 4). Full lines represent the kinetics fit of the experimental data illustrated by circles.



the hot electrons follow the pump pulses⁵⁶. Whereas, the 'slow' component is influenced by the intrinsic relaxation response of the system, primarily dictated by the free-electron temperature (T_e) due to the electron-phonon scattering. In particular, the observed slower temporal component suggests that the relaxation dynamics of the system, occurring at ps time scale, are also influenced by the phonon-phonon scattering and lattice temperature (T_l). This indicates that the temperature of the lattice affects the temporal evolution of the system, especially when nitrides are involved^{56,60}.

Under the same pump fluence and similar intraband excitation (1250 nm NIR pump pulses), Fig. 4b shows an optical switching performance of the metadvice in the NIR-ENZ region when interrogated with 1325 nm probe wavelength. The bleach response maxima occur within $\approx 60 \text{ fs}$ at an ultrafast time scale, followed by a recovery time of 480 fs within an overall temporal switching window of 540 fs. In the Supplementary Note 2, Supplementary Fig. S7b illustrates the transmittance change over time ($\Delta T/T$) corresponding to Fig. 4b. It is noted that our metadvice provides a faster switching response in its effective permittivity than that of homogeneous ENZ thin films and ENZ metasurface counterparts^{15,16,52,56}. In the Supplementary Note 3, we report the slower response time for a single layer of TiN (11 nm) and ITO (32 nm) films, respectively.

We also tested the HMM transient switching response, showcased in Fig. 5, exploring the metadvice behavior under 400 nm pump pulses at higher energy (3.1 eV). Typically, a wavelength range spanning from 325 nm to 500 nm (corresponding to energies between approximately 2.48 eV and 3.82 eV) is employed as the pumping condition for ENZ systems^{60,63}. Within this spectrum, the wavelength of 400 nm (3.1 eV) stands for us as a trade-off choice to investigate the ENZ temporal dynamics at a relatively higher energy for our system. In this context, Fig. 5a presents the reasonable switching response with a recovery time down to 440 fs at 650 nm probe wavelength in the VIS-ENZ region. While in the NIR-ENZ region, the device undergoes a change in dynamic response within 240 fs, followed by a slower recovery time at the order of picoseconds, as shown in Fig. 5b and in Supplementary Fig. S11 in the Supplementary Note 4. In this

scenario, the system is subjected to high-energy pump photons (3.1 eV), resulting in more absorption within the metadvice. Thus, there is a rapid increase in the lattice temperature due to the elevated scattering rate, succeeded by a prolonged thermal heat relaxation^{60,62,64}.

The absorption responses of the HMM, as presented in the inset of Fig. 1a, at pump VIS- (700 nm) and NIR-ENZ (1250 nm) wavelengths, show that the TiN layers exhibit a higher absorption at the VIS-ENZ region with respect to NIR-ENZ. However, at NIR-ENZ (Abs @1250 nm), the ITO layers show stronger absorption. This absorption is significant despite the presence of considerable absorption from TiN, which appears to be lower than its absorption in VIS-ENZ.

Hence, at a longer probe temporal window scale and higher pump energy (3.1 eV), the metadvice possesses a slightly longer recovery time (around $\approx 110 \text{ ps}$), as shown in Supplementary Fig. S11 in the Supplementary Note 4 in comparison to the case when excited by 700 nm (1.7 eV) pump pulses. The long-lived relaxation time in the NIR regions can be attributed to the TiN layers that act as an efficient carrier heating⁶⁰. Thus, we also investigated switching in HMM at the excitation of 400 nm pump pulses (far from the NIR-ENZ region) (see Fig. 5b) and 700 nm (1.7 eV) as shown in Fig. 3f, respectively.

This thermal effect of TiN might result in a higher local temperature in the metamaterial's ITO layers, which induces a change in its permittivity. Therefore, the observed long-tail temporal response in NIR-ENZ, for higher energy, can be due to the heat dissipation in the entire metadvice where the TiN layers act as a heat transducer to the ITO layers influencing its temporal characteristics⁶⁰. We note that by adjusting the pump activation energy at a longer pump wavelength, i.e., 1250 nm (0.9 eV) with low fluence ($1.16 \text{ mJ} \cdot \text{cm}^{-2}$) in NIR-ENZ, the metadvice is capable of fully recovering the transient switching response as shown in Fig. 4b. The latter implies that it is possible to control the ultrafast temporal response in the NIR-ENZ region by controlling the pump wavelength without using high energy, such as UV. The metadvice switching performance in VIS and NIR-ENZ regions for different excitation wavelengths are summarized in Table 1.

Table 1 | Two-color all-optical switching performance of HMM with TiN/ITO layers

Pump λ (nm)	Probe region	Switching time (τ) @ ENZ	Angle of Incident (θ)	Intensity recovery (%)	Fluence ($\text{mJ} \cdot \text{cm}^{-2}$)
400	VIS	440 fs	70°	80	1.40
400	NIR	110 ps ^a	70°	72	1.40
700	VIS	320 fs	0°	≈100	1.40
700	NIR	78 ps ^b	70°	76	1.40
1250	VIS	390 fs	70°	50	1.16
1250	NIR	540 fs	70°	90	1.16

^aSlow relaxation time depicted in Supplementary Fig. S11 in the Supplementary Note 4.

^bSlow relaxation time depicted in Supplementary Fig. S10 in the Supplementary Note 4.

Conclusions

In conclusion, we reported ultrafast switching response in two effective ENZ regions of an HMM based on Si-CMOS-compatible building blocks of TiN/ITO. The results show that the hot electrons dynamics effects are faster in the effective near zero permittivity region of the HMM rather than its thin homogeneous layer counterpart, i.e., TiN (Nitrides), ITO (TCOs), metals, and semiconductors. This opens up a new approach towards realizing tunable and reversible ultrafast all-optical switching at the femtoseconds scale with hybrid solutions. Taking advantage of the optical properties of TiN and ITO at studied wavelengths, we observed fast switching time in VIS as well as NIR-ENZ wavelength regions. This metadvice can function as a double-wavelength switching device, activated by low pump energy, featuring an all-optical modulation response within the 1.8–3.1 THz range.

Our results envision the possibility of particular engineering metamaterials that can potentially be used as fast modulators operating at optical wavelengths. Si-compatible metamaterials can also provide an optimal trade-off between modulation speed and efficient performance in silicon-based photonic systems. Especially, ENZ metamaterials have the potential to launch a new paradigm toward hybrid configuration for ultrafast modulators and photonic-integrated chips.

Methods

Sample preparation

Titanium nitride (TiN) thin films were deposited using the magnetron sputtering technique using Oxford Instruments Plasmalab System 400. Pure Titanium (Ti) was sputtered using a mixture of argon and nitrogen. The addition of nitrogen made the process reactive. The film composition, controlled by the ratio of the argon to nitrogen gas flow, was chosen to be stoichiometric since the plasmonic properties, e.g., the plasmonic figure of merit, are composition-dependent. The process parameters - applied power, pressure, and gas flows were chosen to provide films with the highest value of the figure of merit. All layers were deposited at a temperature of 21 °C with chamber base pressure below 5×10^{-7} Torr. The deposition time was 11 seconds to get 11 nm thick films. Indium-tin-oxide (ITO) was prepared by electron beam evaporation in a custom-made vacuum chamber at the base pressure of 1×10^{-6} mbar. Physical vapor deposition processes obtained ITO layers. For the evaporation of these layers, a vacuum chamber equipped with a telemark 264 electron gun as an evaporation material source, quartz weight for controlling layer evaporation rate and thickness, a heating system for regulating substrates temperature, the system for dosing of oxygen pressure application during evaporation process were used. The ITO deposition process was carried out for 200 °C substrate temperature, under oxygen pressure 7×10^{-5} mbar. ITO material for evaporation consisted of 10% SnO₂ to 90% In₂O₃ by weight.

Optical measurements

The reflectance and transmittance measurements were carried out using a broadband optical source (Energetiq EQ-99XFC LDLS) to excite the samples.

The optical spot is focused on the samples using a Zeiss "Epiplan-Neofluar" 20X objective (NA = 0.4) for both reflectance and transmittance measurements. The response of the samples was coupled to an optical fiber connected to Ocean Optics Flame UV-VIS-NIR spectrometer for the spectral response.

Transient absorption spectroscopy

Ultrafast time-resolved pump-probe spectroscopic measurements were performed using an amplified Ti: sapphire laser system equipped with an optical parametric amplifier (OPA). This system produced less than 100 fs pulses at 1.00 kHz with a center wavelength of 800 nm. Most of the output power (90%) was sent to OPA to generate tunable pump pulses in the UV-Visible to near-infrared spectral regions to excite the samples at the desired wavelength. The remaining 10% of output power travels through a delay line, enabling a controlled time difference between pump and probe pulses. It converts into a broadband probe beam to interrogate the sample in transmission mode. At the same time, the chopper-modulated pump pulse is spectrally as well as temporally overlapped with the probe beam on the sample. At the same time, the detector is triggered to detect every probe pulse and calculate the absorption spectrum. Spectra were collected using a fast optical Multichannel analyzer (OMA) with a de-chirping algorithm. Repetition rates of the pump and probe beams are 500 Hz and 1 kHz, respectively. Therefore, the effect of the pump beam will be observed only in one of the two consecutive probe beams.

Absorption optical power

The optical absorption power per unit volume (P_{abs}) for the metadvice has been calculated using the following relation:

$$P_{abs} = -0.5\omega|E|^2\text{imag}(\epsilon) \quad (1)$$

where ω is the angular frequency, $|E|^2$ represent the magnitude squared of the electric field vector E inside the metadvice, $\text{imag}(\epsilon)$ imaginary part of the permittivities.

Fitting kinetics

The following function has been used to fit all the Kinetics traces for the selected wavelengths by using Surface Explorer (SX) software:

$$S(t) = e^{-\left(\frac{t-t_0}{t_p}\right)^2} * \sum_i A_i e^{-\frac{t-t_0}{t_i}}, t_p = \frac{IRF}{2 \cdot \ln 2} \quad (2)$$

where IRF is the width of the instrument response function (full-width half maximum), t_0 is time zero, A_i and t_i are amplitudes and decay times, respectively.

Data availability

The data that support the findings of this study are available from the corresponding author upon reasonable request.

Received: 23 October 2023; Accepted: 7 May 2024;

Published online: 22 May 2024

References

- Zhu, C., Leung, V. C., Shu, L. & Ngai, E. C.-H. Green internet of things for smart world. *IEEE Access* **3**, 2151–2162 (2015).
- Ono, M. et al. Ultrafast and energy-efficient all-optical switching with graphene-loaded deep-subwavelength plasmonic waveguides. *Nat. Photonics* **14**, 37–43 (2020).
- Chai, Z. et al. Ultrafast all-optical switching. *Adv. Optical Mater.* **5**, 1600665 (2017).
- Dhama, R., Panahpour, A., Pihlava, T., Ghindani, D. & Caglayan, H. All-optical switching based on plasmon-induced enhancement of index of refraction. *Nat. Commun.* **13**, 3114 (2022).
- Caligiuri, V. et al. Near- and mid-infrared graphene-based photonic architectures for ultrafast and low-power electro-optical switching

- and ultra-high resolution imaging. *ACS Appl. Nano Mater.* **3**, 12218–12230 (2020).
6. Kuttruff, J. et al. Ultrafast all-optical switching enabled by epsilon-near-zero-tailored absorption in metal-insulator nanocavities. *Commun. Phys.* **3**, 114 (2020).
 7. Vlasov, Y., Green, W. M. & Xia, F. High-throughput silicon nanophotonic wavelength-insensitive switch for on-chip optical networks. *Nat. Photonics* **2**, 242–246 (2008).
 8. Leuthold, J., Koos, C. & Freude, W. Nonlinear silicon photonics. *Nat. Photonics* **4**, 535–544 (2010).
 9. Shastri, B. J. et al. Photonics for artificial intelligence and neuromorphic computing. *Nat. Photonics* **15**, 102–114 (2021).
 10. Scalora, M., Dowling, J. P., Bowden, C. M. & Bloemer, M. J. Optical limiting and switching of ultrashort pulses in nonlinear photonic band gap materials. *Phys. Rev. Lett.* **73**, 1368 (1994).
 11. Dani, K. M. et al. Subpicosecond optical switching with a negative index metamaterial. *Nano Lett.* **9**, 3565–3569 (2009).
 12. Bleckmann, F. et al. Photochromic switching of fano resonances in metallic photonic crystal slabs. *Adv. Optical Mater.* **2**, 861–865 (2014).
 13. Choi, S. et al. Nanopattern enabled terahertz all-optical switching on vanadium dioxide thin film. *Appl. Phys. Lett.* **98**, 071105 (2011).
 14. Stranks, S. D. et al. Electron-hole diffusion lengths exceeding 1 micrometer in an organometal trihalide perovskite absorber. *Science* **342**, 341–344 (2013).
 15. Kinsey, N. et al. Epsilon-near-zero Al-doped ZnO for ultrafast switching at telecom wavelengths. *Optica* **2**, 616–622 (2015).
 16. Alam, M. Z., De Leon, I. & Boyd, R. W. Large optical nonlinearity of indium tin oxide in its epsilon-near-zero region. *Science* **352**, 795–797 (2016).
 17. Engheta, N. Pursuing near-zero response. *Science* **340**, 286–287 (2013).
 18. Vesseur, E. J. R., Coenen, T., Caglayan, H., Engheta, N. & Polman, A. Experimental verification of $n=0$ structures for visible light. *Phys. Rev. Lett.* **110**, 013902 (2013).
 19. Wu, J., Xie, Z. T., Sha, Y., Fu, H. & Li, Q. Epsilon-near-zero photonics: infinite potentials. *Photonics Res.* **9**, 1616–1644 (2021).
 20. Bohn, J. et al. All-optical switching of an epsilon-near-zero plasmon resonance in indium tin oxide. *Nat. Commun.* **12**, 1017 (2021).
 21. Vezzoli, S. et al. Optical time reversal from time-dependent epsilon-near-zero media. *Phys. Rev. Lett.* **120**, 043902 (2018).
 22. Xie, Z. T., Wu, J., Fu, H. & Li, Q. Tunable electro- and all-optical switch based on epsilon-near-zero metasurface. *IEEE Photonics J.* **12**, 1–10 (2020).
 23. Miscuglio, M. et al. Approximate analog computing with metatronic circuits. *Commun. Phys.* **4**, 196 (2021).
 24. Amin, R. et al. Sub-wavelength GHz-fast broadband ITO Mach-Zehnder modulator on silicon photonics. *Optica* **7**, 333–335 (2020).
 25. Niu, X., Hu, X., Chu, S. & Gong, Q. Epsilon-near-zero photonics: a new platform for integrated devices. *Adv. Optical Mater.* **6**, 1701292 (2018).
 26. Galiffi, E. et al. Photonics of time-varying media. *Adv. Photonics* **4**, 014002–014002 (2022).
 27. Neira, A. D., Wurtz, G. A. & Zayats, A. V. All-optical switching in silicon photonic waveguides with an epsilon-near-zero resonant cavity. *Photonics Res.* **6**, B1–B5 (2018).
 28. Navarro-Arenas, J., Parra, J. & Sanchis, P. Ultrafast all-optical phase switching enabled by epsilon-near-zero materials in silicon. *Opt. Express* **30**, 14518–14529 (2022).
 29. Sha, Y., Xie, Z. T., Wu, J., Fu, H. & Li, Q. All-optical switching in epsilon-near-zero asymmetric directional coupler. *Sci. Rep.* **12**, 17958 (2022).
 30. Minzioni, P. et al. Roadmap on all-optical processing. *J. Opt.* **21**, 063001 (2019).
 31. Lau, K. Y., Yang, Y., Zhao, D., Liu, X. & Qiu, J. Tunable optical nonlinearity of indium tin oxide for optical switching in epsilon-near-zero region. *Nanophotonics* **11**, 4209–4219 (2022).
 32. Zhang, Z., Liu, J., Hao, Q. & Liu, J. Sensitive saturable absorber and optical switch of epsilon-near-zero medium. *Appl. Phys. Express* **12**, 065504 (2019).
 33. Poddubny, A., Iorsh, I., Belov, P. & Kivshar, Y. Hyperbolic metamaterials. *Nat. Photonics* **7**, 948–957 (2013).
 34. Guo, Z., Jiang, H. & Chen, H. Hyperbolic metamaterials: From dispersion manipulation to applications. *J. Appl. Phys.* **127**, 071101 (2020).
 35. Pianelli, A. et al. Active control of dielectric singularities in indium-tin-oxides hyperbolic metamaterials. *Sci. Rep.* **12**, 16961 (2022).
 36. Pianelli, A. et al. Graphene-based hyperbolic metamaterial as a switchable reflection modulator. *Opt. Express* **28**, 6708–6718 (2020).
 37. Caligiuri, V., Dhama, R., Sreekanth, K., Strangi, G. & De Luca, A. Dielectric singularity in hyperbolic metamaterials: the inversion point of coexisting anisotropies. *Sci. Rep.* **6**, 1–10 (2016).
 38. Wu, F. et al. Redshift gaps in one-dimensional photonic crystals containing hyperbolic metamaterials. *Phys. Rev. Appl.* **10**, 064022 (2018).
 39. Wu, F., Chen, M. & Xiao, S. Wide-angle polarization selectivity based on anomalous defect mode in photonic crystal containing hyperbolic metamaterials. *Opt. Lett.* **47**, 2153–2156 (2022).
 40. Maas, R., Parsons, J., Engheta, N. & Polman, A. Experimental realization of an epsilon-near-zero metamaterial at visible wavelengths. *Nat. Photonics* **7**, 907–912 (2013).
 41. Habib, M., Briukhanova, D., Das, N., Yildiz, B. C. & Caglayan, H. Controlling the plasmon resonance via epsilon-near-zero multilayer metamaterials. *Nanophotonics* **9**, 3637–3644 (2020).
 42. Boyd, R. W. & Sipe, J. E. Nonlinear optical susceptibilities of layered composite materials. *JOSA B* **11**, 297–303 (1994).
 43. Lepeshkin, N. N., Schweinsberg, A., Piredda, G., Bennink, R. S. & Boyd, R. W. Enhanced nonlinear optical response of one-dimensional metal-dielectric photonic crystals. *Phys. Rev. Lett.* **93**, 123902 (2004).
 44. Ciattoni, A., Rizza, C. & Palange, E. Extreme nonlinear electrodynamics in metamaterials with very small linear dielectric permittivity. *Phys. Rev. A* **81**, 043839 (2010).
 45. Rashed, A. R., Yildiz, B. C., Ayyagari, S. R. & Caglayan, H. Hot electron dynamics in ultrafast multilayer epsilon-near-zero metamaterials. *Phys. Rev. B* **101**, 165301 (2020).
 46. Kaipurath, R. et al. Optically induced metal-to-dielectric transition in epsilon-near-zero metamaterials. *Sci. Rep.* **6**, 1–7 (2016).
 47. Xie, Z. T., Sha, Y., Wu, J., Fu, H. & Li, Q. Ultrafast dynamic switching of optical response based on nonlinear hyperbolic metamaterial platform. *Opt. Express* **30**, 21634–21648 (2022).
 48. Hu, F., Jia, W., Meng, Y., Gong, M. & Yang, Y. High-contrast optical switching using an epsilon-near-zero material coupled to a Bragg microcavity. *Opt. Express* **27**, 26405–26414 (2019).
 49. Kim, T. Y. et al. General strategy for broadband coherent perfect absorption and multi-wavelength all-optical switching based on epsilon-near-zero multilayer films. *Sci. Rep.* **6**, 22941 (2016).
 50. Suresh, S. et al. Enhanced nonlinear optical responses of layered epsilon-near-zero metamaterials at visible frequencies. *ACS Photonics* **8**, 125–129 (2020).
 51. Genchi, D., Balasa, I. G., Cesca, T. & Mattei, G. Tunable third-order nonlinear optical response in ϵ -near-zero multilayer metamaterials. *Phys. Rev. Appl.* **16**, 064020 (2021).
 52. Alam, M. Z., Schulz, S. A., Upham, J., De Leon, I. & Boyd, R. W. Large optical nonlinearity of nanoantennas coupled to an epsilon-near-zero material. *Nat. Photonics* **12**, 79–83 (2018).
 53. Clerici, M. et al. Controlling hybrid nonlinearities in transparent conducting oxides via two-colour excitation. *Nat. Commun.* **8**, 15829 (2017).
 54. Fruhling, C., Ozlu, M. G., Saha, S., Boltasseva, A. & Shalaev, V. M. Understanding all-optical switching at the epsilon-near-zero point: a tutorial review. *Appl. Phys. B* **128**, 34 (2022).
 55. Kinsey, N., DeVault, C., Boltasseva, A. & Shalaev, V. M. Near-zero-index materials for photonics. *Nat. Rev. Mater.* **4**, 742–760 (2019).
 56. Diroll, B. T., Saha, S., Shalaev, V. M., Boltasseva, A. & Schaller, R. D. Broadband ultrafast dynamics of refractory metals: Tin and zrn. *Adv. Optical Mater.* **8**, 2000652 (2020).

57. Groeneveld, R. H. M., Sprik, R. & Lagendijk, A. Femtosecond spectroscopy of electron-electron and electron-phonon energy relaxation in ag and au. *Phys. Rev. B* **51**, 11433–11445 (1995).
58. Dhama, R., Habib, M., Rashed, A. R. & Caglayan, H. Unveiling long-lived hot-electron dynamics via hyperbolic meta-antennas. *Nano Lett.* **23**, 3122–3127 (2023).
59. Schirato, A., Maiuri, M., Cerullo, G. & Della Valle, G. Ultrafast hot electron dynamics in plasmonic nanostructures: experiments, modelling, design. *Nanophotonics* **12**, 1–28 (2023).
60. Rotta Loria, S. et al. Unfolding the origin of the ultrafast optical response of titanium nitride. *Adv. Optical Mater.* **11**, 2300333 (2023).
61. Judek, J. et al. Ultrafast optical properties of stoichiometric and non-stoichiometric refractory metal nitrides tinx, zrnx, and hfnx. *Opt. Express* **32**, 3585–3596 (2024).
62. George, H. et al. Nonlinearities and carrier dynamics in refractory plasmonic tin thin films. *Optical Mater. Express* **9**, 3911–3924 (2019).
63. Saha, S. et al. Engineering the temporal dynamics of all-optical switching with fast and slow materials. *Nat. Commun.* **14**, 5877 (2023).
64. Norris, P. M. et al. Femtosecond pump–probe nondestructive examination of materials. *Rev. Sci. Instrum.* **74**, 400–406 (2003).

Acknowledgements

We acknowledge the financial support of the European Research Council (Starting Grant project aQUARiUM; Agreement No. 802986), Academy of Finland Flagship Programme (PREIN), (320165). All authors thank Dr. Urszula Chodorow for her support in ellipsometric measurements, Dr. Antti Tukiainen for the Hall measurements, and Jesse Pietila for the SEM cross-section of the HMM. J.J. thanks to the POB FOTECH-3 project entitled "Plasmons and polaritons on nanostructured surfaces of IVb metal nitrides" granted by the Warsaw University of Technology within "The Excellence Initiative - Research University" program.

Author contributions

A.P. conceived the idea, performed the design and simulations, prepared the first draft of the manuscript, and, with the support of A.P., R.D., and H.C., wrote the final version of the manuscript. A.P. prepared the figures, and A.P. and R.D. analyzed the data. R.D. conducted the experiments with the support of A.P. J.J., and R.M. fabricated the samples. A.P., R.D., and

H.C. checked the results thoroughly and reviewed the manuscript. H.C. supervised the project.

Competing interests

The authors declare no competing interests.

Additional information

Supplementary information The online version contains supplementary material available at <https://doi.org/10.1038/s42005-024-01654-1>.

Correspondence and requests for materials should be addressed to Humeyra Caglayan.

Peer review information *Communications Physics* thanks Jiaye Wu and the other, anonymous, reviewer(s) for their contribution to the peer review of this work. A peer review file is available.

Reprints and permissions information is available at <http://www.nature.com/reprints>

Publisher's note Springer Nature remains neutral with regard to jurisdictional claims in published maps and institutional affiliations.

Open Access This article is licensed under a Creative Commons Attribution 4.0 International License, which permits use, sharing, adaptation, distribution and reproduction in any medium or format, as long as you give appropriate credit to the original author(s) and the source, provide a link to the Creative Commons licence, and indicate if changes were made. The images or other third party material in this article are included in the article's Creative Commons licence, unless indicated otherwise in a credit line to the material. If material is not included in the article's Creative Commons licence and your intended use is not permitted by statutory regulation or exceeds the permitted use, you will need to obtain permission directly from the copyright holder. To view a copy of this licence, visit <http://creativecommons.org/licenses/by/4.0/>.

© The Author(s) 2024